Chapter 3 Mesoporous Silica (MS) Films

3-1. Fabricating various nanostructures of MS film

Molecularly templated mesoporous silica (**MS_{as}**) films are initially spin-coated on silicon wafers using sol-gel-prepared precursors that contain different organic templates (cetyltrimethylammonium bromide (**CTAB),** polyoxyethylene cetyl ether **(Brij-56)**, and Triblock copolymer Pluronic P-123 (**P123**)) for controlling the pore-size [12], followed by baking at 110°C for one hour [15]. MS materials are synthesized via a liquid-crystal mechanism [12], in which the nanostructures are formed by molecular self-assembly aggregation. The organic template is removed by furnace annealing (**FA**) in nitrogen at 400-500 ^{0}C for one hour or by ozone ashing (**OA**) at 250-350 ^{0}C for 2-5 min respectively, yielding **MS** films [22]. Different calcination processes for removing organic templates are used to modulate the thickness of the pore-wall. The spatial dimensions of the MS matrix are characterized by Kr absorption/desorption and X-ray diffraction [15] (XRD)**.** Some mesoporous silica films are treated with hexamethyldisilazane (**HMDS**) vapor at 160°C to modify the Si-OH groups on pore surfaces via a silylating reaction [14], denoted as **MS_{HMDS}**. Post-annealing (**PA)** was performed in nitrogen at 350 ^{0}C for 1 h, to degas the absorbed moisture in the MS matrix. For comparison, thermal silicon oxide (**SiO_2**) was also deposited. Fourier transformation infrared spectroscopy (**FTIR**) and thermal desorption spectra (**TDS**) were applied to analyze the chemical bonds and moisture desorption of those mesoporous silica films at various aging times and PA treatment. Room-temperature PL for all samples was obtained using an excitation He-Cd laser (325 nm) at 300 W/cm^2. All films are ~300 nm thickness.

3-2. Material analysis of MS films

3-2.1 TEM image of MS films

A cross-sectional transmission electron microscopic (**TEM**) image of MS films (Brij-56 used), shown in the inset of Fig. 3-1(a), reveals that such films consist of well-aligned mesochannels parallel to the Si surface.

3-2.2 Kr absorption/desorption isotherms of MS films

Kr absorption/desorption isotherms for MS films synthesized using precursors with various templates (**CTAB, Brij-56**, and **P123**), presented in Fig. 3-1 (a), demonstrate an adjustable pore-size $\mathbf{D_p}$ from 2.0 to 5.0 nm. The calcination process is of FA at 400-500 ^{0}C.

3-2.3 X-ray diffraction patterns of MS films

The X-ray diffraction patterns for the samples in Fig. 3-1 (a), depicted in Fig. 3-1 (b), further yield the pore-to-pore distance, $\mathbf{D_{PTP}}$, and an almost constant pore-wall $\mathbf{S_P}$ of 1.3 ± 0.1 nm**.**

3-2.4 Measurements of different calcination processes

The measurements were taken of MS films that were undergoing different calcination processes (FA at 450 ^{0}C, FA at 400 ^{0}C, OA at 300 ^{0}C, and OA at 275 ^{0}C) , as shown in Figs. 3-1 (c, d), indicate variable S_P from 1.2 to 1.9 ± 0.1 nm and D_P of about 5.0 nm (P123 used). Those results in Fig. 3-1 thus open the feasibility in controlling nanostructures of MS films. Afterwards, all experiments are conducted using MS films with a pore-size of ~5 nm and a pore-wall of ~1.8 nm excepting the PL studying associated with nanostructures of the MS matrix (in Fig. 3-4).

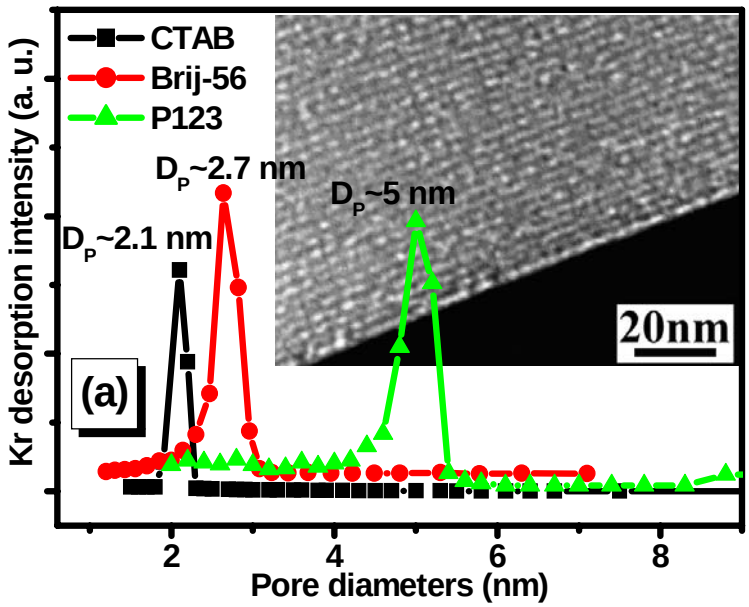

Fig. 3-1: (a): Kr absorption/desorption isotherms of MS films with various templates. The inset in Fig. 3-1(a) shows a cross-sectional TEM plot of a typical MS film.

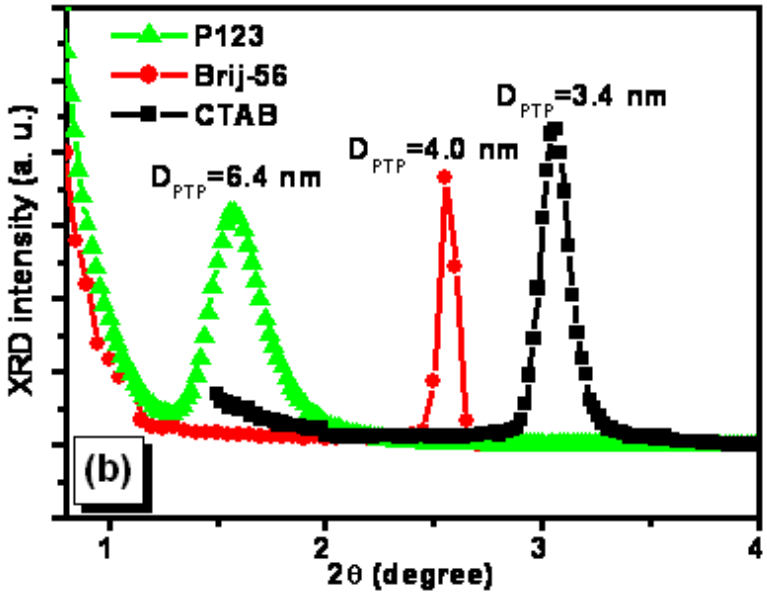

Fig. 3-1: (b): X-ray diffraction patterns for MS films synthesized using precursors with various organic templates.

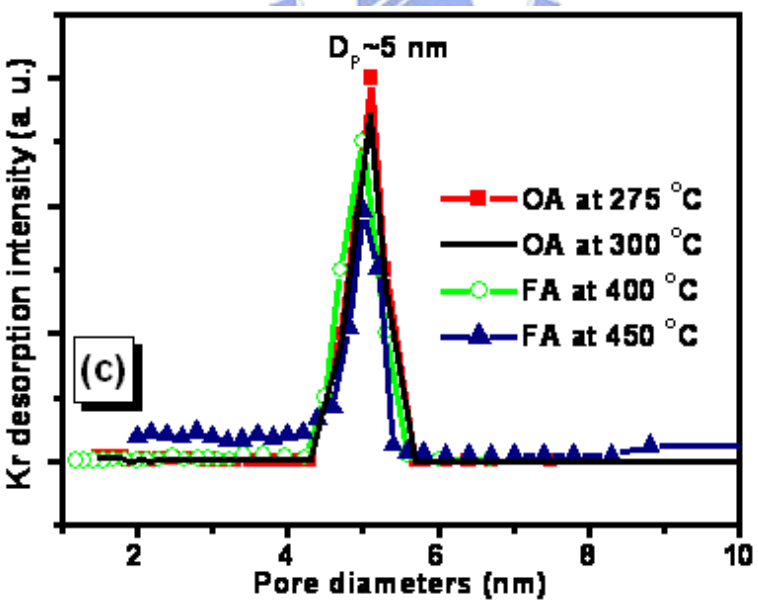

Fig. 3-1: (c): Kr absorption/desorption isotherms for MS films that are undergoing different calcination processes.

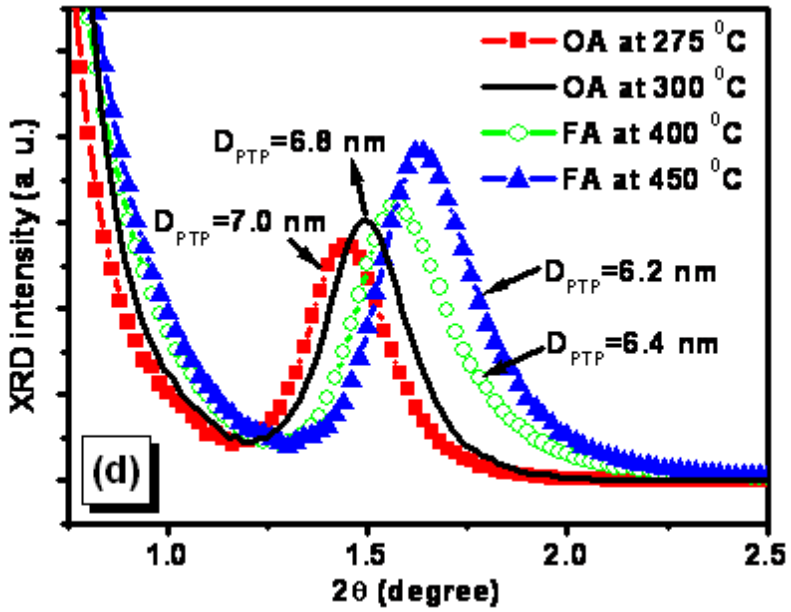

Fig. 3-1: (d): X-ray diffraction patterns for MS films that are undergoing different calcination processes. The pore-wall (S_P) is determined using the formula of $S_P=D_{PTP}-D_P$, where D_{PTP} is $2\times d_{spacing}/\sqrt{3}$, based on the assumption that the mesochannels are packed with hexagonal symmetry, and $d_{spacing}$ is measured by XRD 2θ scanning.

3-3. Room-temperature PL spectra of MS films

3-3.1 PL spectra of MS films

Three peaks (415, 460 and 580 nm) on the PL spectrum of as-calcined MS films (Fig. 3-2) are attributable to the radiative defects of two-fold-coordinated silicon lone-pair center-related species (SLP) [:Si:] [17-18], neutral oxygen vacancies (NOV) [≡Si-Si≡] [16-17], and nonbridging oxygen hole centers (NBOHC) [≡Si-O•] [9], respectively.

3-3.2 PL-related bonds of MS films and silylation reaction

Inset (a) in Fig. 3-2 schematically depicts the PL-related bonds in the silica matrix. Figure 3-2 also reveals a significant decline on PL from MS after 4 h of aging. (See the curves of MS+4h and as-calcined MS.) Applying PA to MS films actually returns the PL strength to that of as-calcined MS. (See the curves of MS+PA, and the as-calcined MS in Fig. 3-2.)

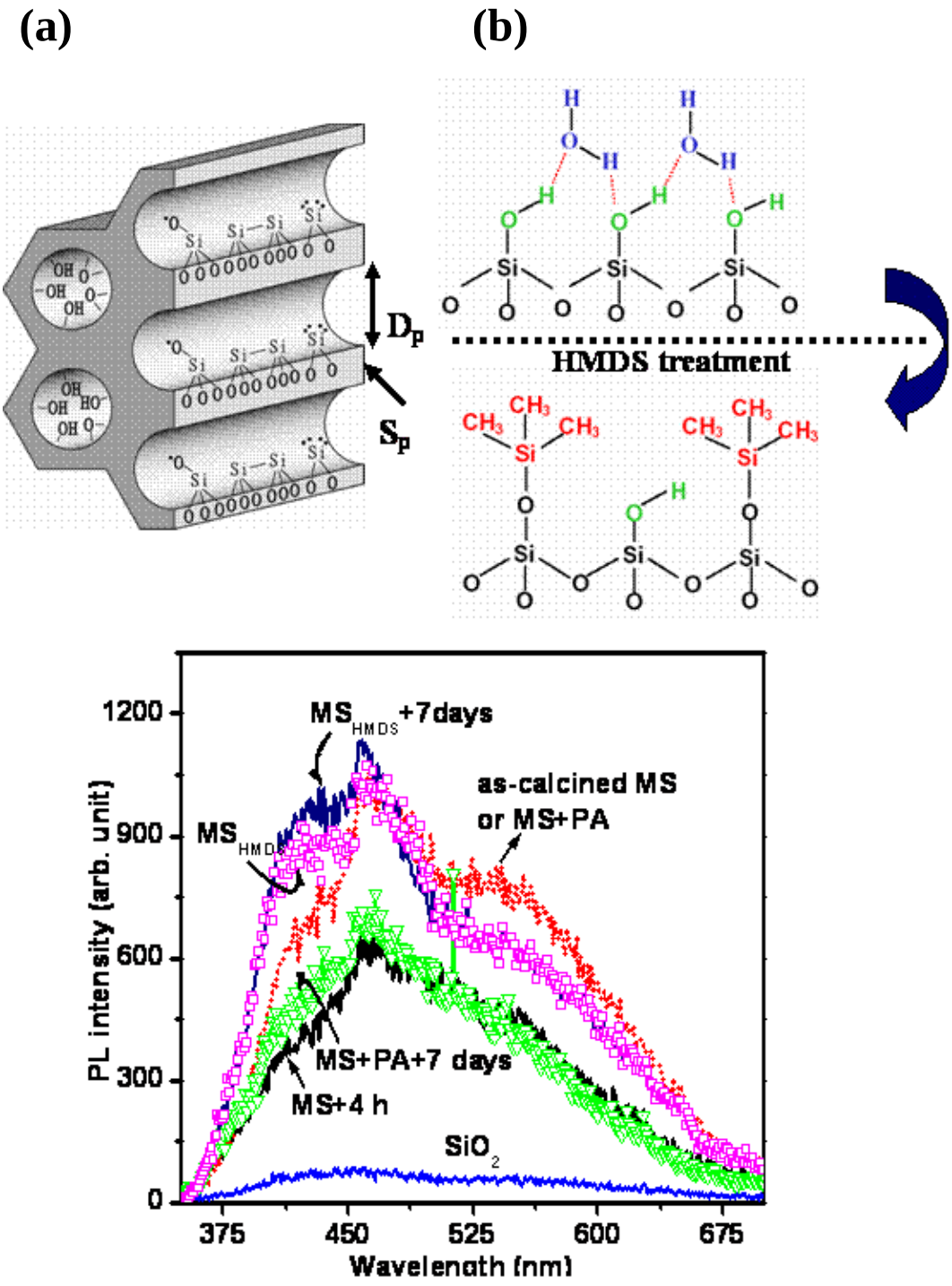

Fig. 3-2: PL spectra of MS and MS_{HMDS} at various aging time, followed, or not followed by, PA at 350 ^{0}C. PL of SiO_2 is also shown for comparison. Inset (a) schematically represents PL-related bonds on the porechannel and inset (b) depicts the chemical formula for the silylation reaction.

3-3.3 FTIR and TDS spectra of MS films

The absence of the template-related (2830-3040 cm^{-1}) peak on the FTIR spectrum for as-calcined MS films, shown on Fig. 3-3 (a), indicates the removal of organic templates within MS_{as}. After calcination, numerous silanol groups on the surfaces of the porechannels attract moisture, responding to the H_2O-related peak (3200-3750 cm^{-1}) of the FTIR curve (MS+4 h) for MS, after 4 h of aging, plotted on Fig. 3-3 (a). It will screen radiative recombination centers and then form non-radiative paths, eventually lowering the PL strength of MS, as shown in Fig. 3-2, and observed by Chang et al. [23].

TDS in Fig. 3-3 (b) shows the degassing behaviors of H_2O-related species from MS films, clearly indicating that PA at 350 ^0C removes these species from the MS matrix. However, annealed MS films still have hydrophilic characteristics and absorb moisture again, with associated degradation of the PL to the level obtained with MS after aging, as revealed by the curve (MS+PA+7 days) in Fig. 3-2 for annealed MS after aging for 7 days.

Our earlier work demonstrated that the hydrophobicity of a calcined MS film was improved by HMDS vapor post-treatment [15]. The presence of Si-C and C-H peaks on the FTIR spectra for HMDS-treated MS films, shown in Fig. 3-3 (a), demonstrates that the hydrophilic groups of Si-OH have been replaced by the hydrophobic groups of $Si-(CH_3)_3$. This silylating reaction, the formula of which is presented in inset (b) of Fig. 3-2, causes MS_{HMDS} to absorb a little moisture, as evidenced by the low H_2O-related TDS intensity for MS_{HMDS}, as shown in Fig. 3-3 (b) The PL strength of MS_{HMDS} is thus the same as that of the as-calcined MS, as shown on Fig. 3-2. The PL spectrum of MS_{HMDS}, presented on Fig. 3-2, was found to coincide with that of as-calcined MS due to the fact that the chemical structures of three radiation defects are unaffected by the silylating reaction, as depicted in the insets (a, b) of Fig. 3-2. Unlike PA treatment for MS, the HMDS treatment is an irreversible process for reducing moisture absorption, as determined from observations of the PL strength of MS_{HMDS} with a long-term seven-day stability. (See the curve of MS_{HMDS}+7days in Fig. 3-2.) The CH_4-related TDS for MS_{HMDS} films starts to increase clearly from a high temperature of 400 ^0C, suggesting that such films have highly thermally stable PL intensity.

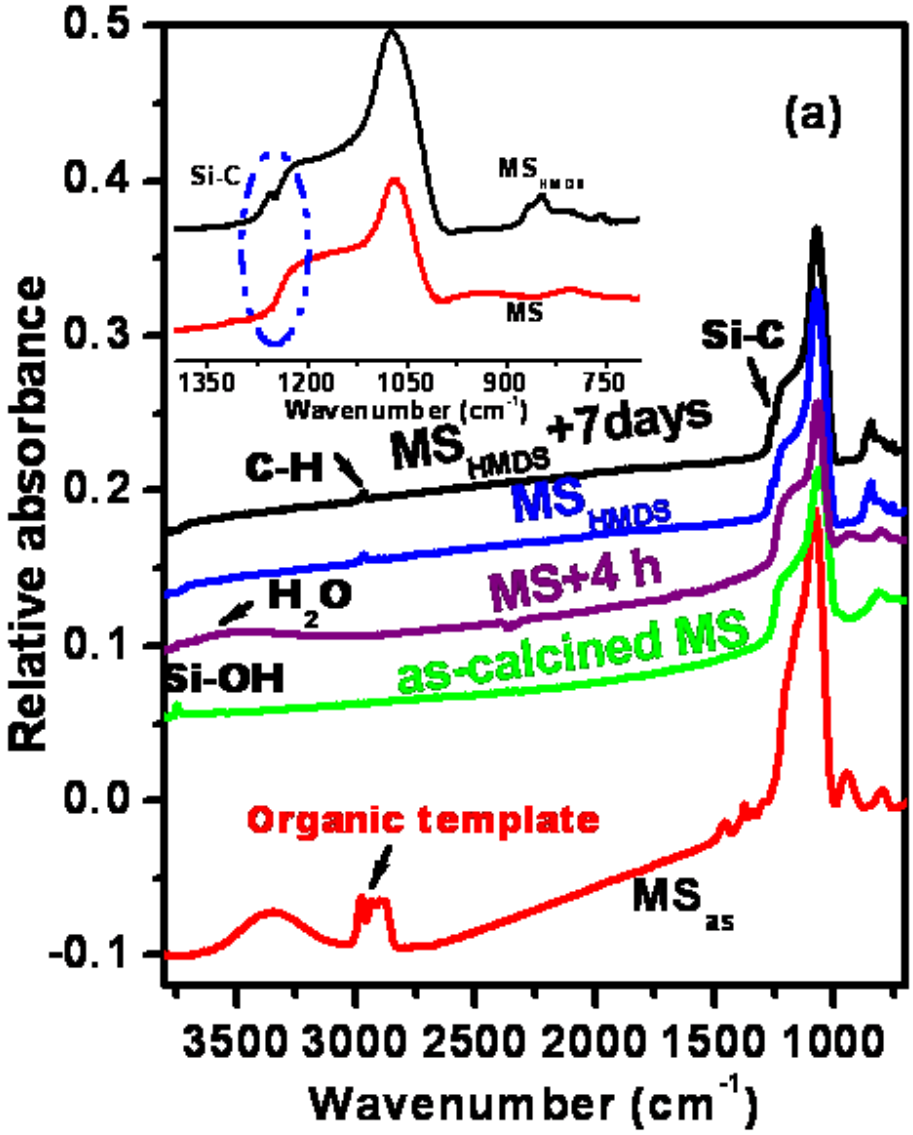

Fig. 3-3: (a): FTIR spectra of MS_{as}, MS and MS_{HMDS} at various aging time. The inset locally magnifies the FTIR spectra around the Si-C peak (1258 cm^{-1}) for MS and MS_{HMDS}.

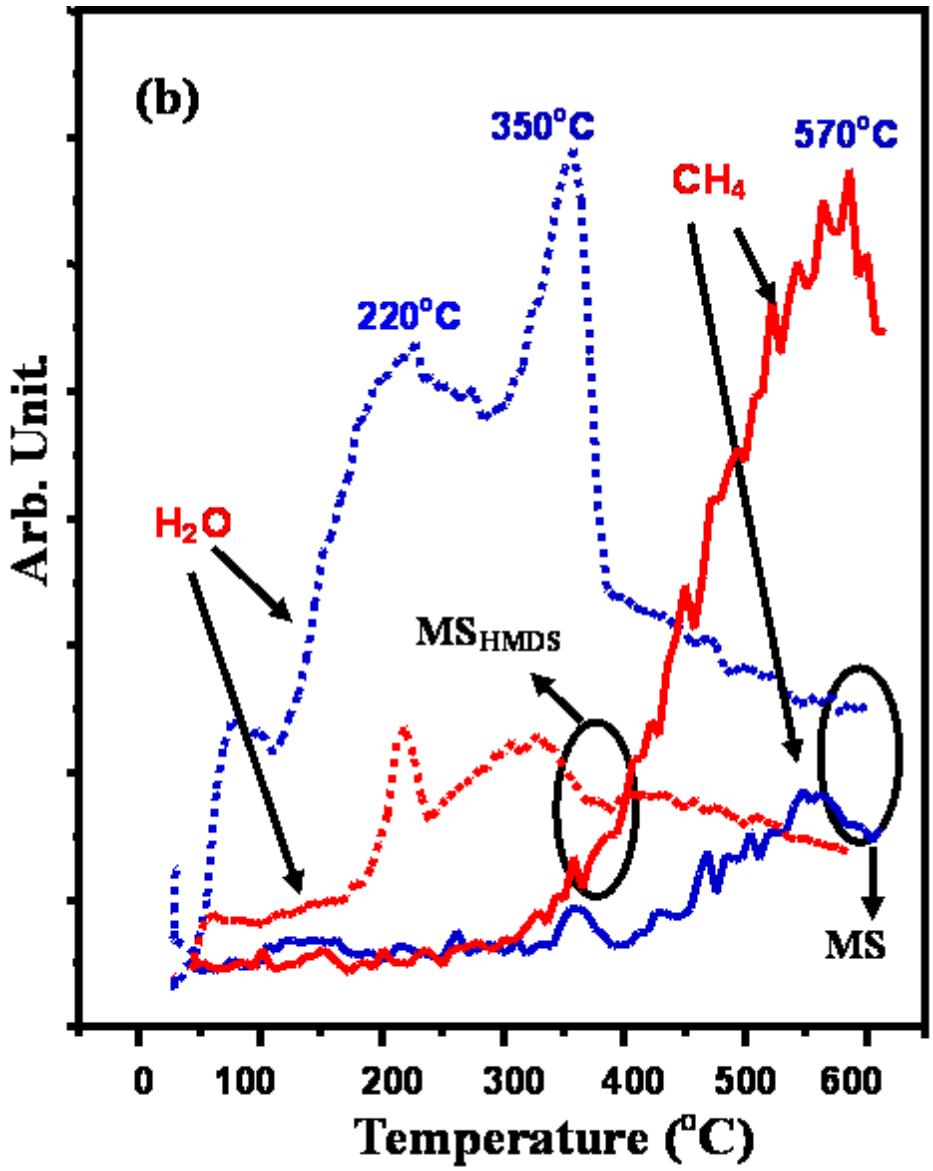

Fig. 3-3: (b): H_2O-related and CH_4-related TDS for MS and MS_{HMDS}.

3-3.4 PL spectra for MS with different pore-size and pore-wall

The structures of the MS matrix determine both the total surface areas and the nanoscaled environments contributed by the porechannels, and so affect the PL behaviors. Based on the assumption that the MS matrix has a hexagonal self-assembled structure, Fig. 3-4 (a) plots the simulated normalized areas A_{MS} of the porechannels as functions of pore-size D_p and pore-wall S_p , predicting that A_{MS} increases as D_p and S_p decreases.

Figure 3-4 (b) reveals that the SLP-related PL from MS films increases more rapidly than the PL associated with other peaks, as the pore-size decreases, even though the overall surface-area in MS increases. The high curvature associated with the small pores seriously stresses the pores' surfaces, causing more bonds to break (or defects to be formed). The structure of the chemical bonds on the surfaces of the porechannels indicates that most defects, generated by the shrinkage of pores, are abundant lone-pair Si species rather than oxygen-related defects, explaining dependence of SLP-related and NBOHC-related PL on the pore-size. NOV-related PL is associated with rich-Si-modulated-SiO_2 (Si_n/SiO_m) composites and the MS matrix is doped with no external impurities, so the PL varies slightly with the pore-size. According to the theory which is proposed by M. V. Wolkin et al. [24], quantum-confinement-related (QC) PL from the nanoscaled Si_n/SiO_m composites or Si nanodots bonded with pore-walls [Si=O] contributes to spectra above 590 nm (or at a photonic energy of below 2.1 eV), and so is weakly involved in the emission of blue-white light.

Figure 3-4 (c) further reveals that the entire strength of PL from the MS films increases as the pore-wall decreases, since the pore-size (or intrpore environments) in MS matrix does not change, but the number of reactive surfaces associated with the pore-wall increases as the pore-wall becomes thinner.

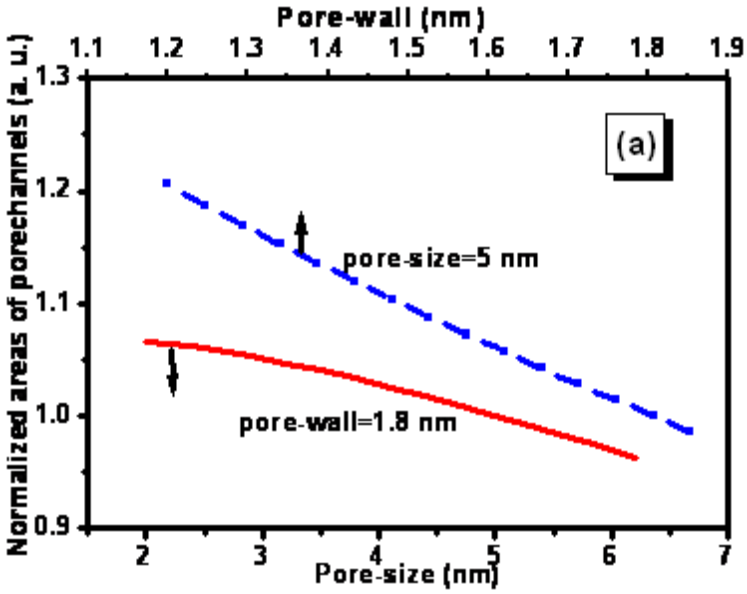

Fig. 3-4: (a): Normalized surface areas of porechannels as functions of pore-size and pore-wall. The normalized factor is the total surface area of the porechannels for MS with pore-size=5 nm, and pore-wall=1.8 nm.

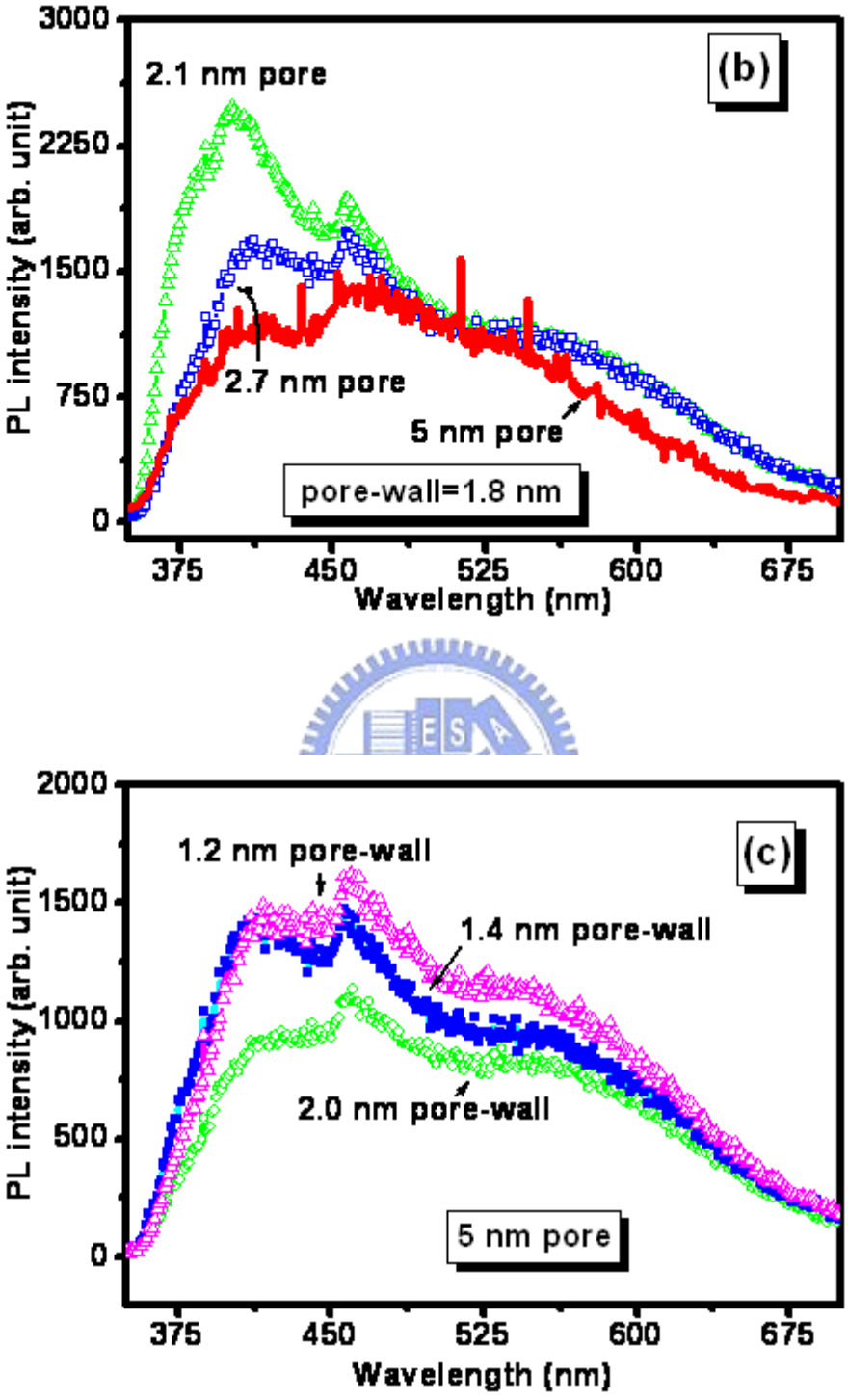

Fig. 3-4: (b): PL spectra for MS with different pore-sizes and with pore-wall=1.8 nm. (c): PL spectra for MS with various pore-wall and with pore-size=5.0 nm.

3-4. Conclusion

The luminescence behaviors of mesoporous silica films were studied with reference to self-assembled pore nanostructures. Reducing pore-size and pore-wall can increase the total area of the pore-surfaces (and, therefore, the number of radiative recombination centers) within the MS matrix, enhancing PL efficiency. Moreover, the number of silianol groups on pore-surfaces, which absorb moisture and degrade the PL of the MS films, is greatly reduced by silylating MS with hydrophobicity, yielding long-term stable luminescence. The quantum-efficiency of photoluminescence of the MS films is measured about 5.0×10^{-4}.